CHEMISTRY OF MATERIALS
Article

*Chem. Mater.* **2010,** *22,* 3389–3398 3389
DOI:10.1021/cm100189t

# Influence of Alkyl Side-Chain Length on the Performance of Poly(3-alkylthiophene)/Polyfluorene All-Polymer Solar Cells

Bettina Friedel,* Christopher R. McNeill, and Neil C. Greenham

*Cavendish Laboratory, Department of Physics, University of Cambridge, J. J. Thomson Avenue, Cambridge CB3 0HE, United Kingdom*

*Received January 21, 2010. Revised Manuscript Received April 20, 2010*

We have investigated the influence of the alkyl side-chain length of poly(3-alkylthiophene) (P3AT) on the performance of all-polymer blend photovoltaic devices with the polyfluorene copolymer F8TBT (poly((9,9-dioctylfluorene)-2,7-diyl-alt-[4,7-bis(3-hexylthien-5-yl)-2,1,3-benzothiadiazole]-2′,2″-diyl)) used as the electron acceptor. Butyl, hexyl, octyl, and decyl side-chains have been studied, with clear trends in the device performance observed. The properties of the unblended polythiophene are first reported, namely their thermal, photophysical, electrochemical, and morphological characteristics. The observed trends in photovoltaic device performance are interpreted in terms of the complex interplay between energy level offsets, blend morphology and charge carrier mobility. Device performance is especially sensitive to the annealing temperature employed that influences both the recrystallization of P3AT and the coarsening of phase separation. Poly(3-hexylthiophene) (P3HT) is found to be the optimum P3AT studied, because of the appropriate energy level offsets with F8TBT and the fact that P3HT recrystallization occurs before significant phase separation.

## Introduction

Semiconducting conjugated polymers as the active component in photovoltaic devices and photodetectors have received increasing attention because of their potential to deliver large-area devices at low cost through solution processing, allowing the material to be deposited on virtually any surface, including plastic or fiber-based flexible substrates.[1,2] Compared to commonly used inorganic material systems only very thin films (on the order of 100 nm) are required and so less material is needed, because of the high optical absorption coefficients. Another important benefit is the flexibility afforded by chemical synthesis in tuning the optical absorption range of the materials, which allows a large part of the solar spectrum to be covered.[3] Photocurrent generation processes in organic devices are markedly different from inorganic cells, providing challenges for understanding and optimizing device performance. Although in inorganic devices photogenerated electrons and holes are easily separated, in conjugated polymers a tightly bound exciton (binding energy ~0.4 eV [4]) is generated that has to travel to a donor−acceptor interface by diffusion in order to dissociate. Even after exciton dissociation at a donor−acceptor interface, the geminate electron−hole pair may remain bound at the interface due to the mutual Coulombic attraction of the carriers and the low dielectric constant of organic materials. The efficiency of separation of interfacial charge separation is strongly dependent upon temperature, electric field and the initial charge−pair separation distance.[5] Recently it has also been suggested that the energy level offset between donor and acceptor can also strongly influence the efficiency of charge separation.[6] Because of the low exciton diffusion length of conjugated polymers ($\leq$10 nm[7,8]), efficient organic solar cells employ a blended or bulk-heterojunction (BHJ) architecture.[9,10] The active layer in a polymer BHJ solar cell is characterized by a mixture of donor and acceptor where the donor is typically a conjugated polymer and the acceptor may be another conjugated polymer,[11] a fullerene derivative,[12] or an inorganic nanocrystal.[13] The domains of

*Corresponding author. Email address: bf245@cam.ac.uk.

(1) Al-Ibrahim, M.; Roth, H. K.; Sensfuss, S. *Appl. Phys. Lett.* **2004**, *85*, 1481–1483.
(2) Greulich-Weber, S.; Friedel, B.; Zoeller, M; PCT Int. Appl. **2008**.
(3) Hoppe, H.; Sariciftci, N. S. *Adv. Polym. Sci.* **2008**, *214*, 1–86.
(4) Koster, L. J. A.; Mihailetchi, V. D.; Blom, P. W. M. *Appl. Phys. Lett.* **2006**, *88*, 093511.
(5) Mihailetchi, V. D.; Koster, L. J. A.; Hummelen, J. C.; Blom, P. W. M. *Phys. Rev. Lett.* **2004**, *93*, 216601.
(6) Ohkita, H.; Cook, S.; Astuti, Y.; Duffy, W.; Tierney, S.; Zhang, W.; Heeney, M.; McCulloch, I.; Nelson, J.; Bradley, D. D. C.; Durrant, J. R. *J. Am. Chem. Soc.* **2008**, *103*, 3030–3042.
(7) Markov, D. E.; Amsterdam, E.; Blom, P. W. M.; Sieval, A. B.; Hummelen, J. C. *J. Phys. Chem. A* **2005**, *109*, 5266.
(8) Shaw, P. E.; Ruseckas, A.; Samuel, I. D. W. *Adv. Mater.* **2008**, *20*, 3516–3520.
(9) Halls, J. J. M.; Walsh, C. A.; Greenham, N. C.; Marseglia, E. A.; Friend, R. H.; Moratti, S. C.; Holmes, A. B. *Nature* **1995**, *376*, 498–500.
(10) Yu, G.; Gao, J.; Hemmelen, J. C.; Wudl, F.; Heeger, A. J. *Science* **1995**, *270*, 1789–1791.
(11) McNeill, C. R.; Abrusci, A.; Zaumseil, J.; Wilson, R.; McKiernan, M. J.; Halls, J. J. M.; Greenham, N. C.; Friend, R. H. *Appl. Phys. Lett.* **2007**, *90*, 193506.
(12) Ma, W.; Yang, C.; Gong, X.; Lee, K.; Heeger, A. J. *Adv. Funct. Mater.* **2005**, *15*, 1617–1622.
(13) Sun, B.; Marx, E.; Greenham, N. C. *Nano Lett.* **2003**, *3*, 961–963.


Published on Web 05/07/2010

the separated phases have to be small enough to facilitate exciton dissociation, but sufficiently extended and interconnected enough to ensure charge collection. Recent work has also shown that domain size also has a strong influence on the interfacial charge separation process, with coarser domains improving the probability of charge separation.[14,15] The optimization of morphology therefore has to balance the requirements of exciton dissociation, charge separation, and charge transport. Control of nanomorphology in solution-processed blends is challenging, however, with morphology depending strongly on a number of factors including deposition method, solvent, miscibility, composition ratio, surface energies of polymers and substrate material, temperature or postdeposition treatments.[16−19]

This report is focused on a polymer/polymer system involving regioregular poly(3-alkylthiophenes) (RR-P3ATs) acting as the electron donor and the polyfluorene copolymer poly((9,9-dioctylfluorene)-2,7-diyl-alt-[4,7-bis(3-hexylthien-5-yl)-2,1,3-benzothiadiazole]-2′,2″-diyl) (F8TBT) as the electron acceptor. The polymer/polymer system P3HT:F8TBT has been intensively studied and we have recently demonstrated power conversion efficiencies of nearly 2%[11] for devices based on this blend. The high mobilities within P3HT are thought to be mainly responsible for the success of P3HT:F8TBT devices, because efficient charge separation is promoted, helping to overcome the problem of geminate recombination that is prevalent in all-polymer blend devices. In this study, we investigate if alteration of the alkyl chain length of the polythiophene can deliver further improvements in device performance. Similar studies have already been performed on pure poly(3-alkylthiophene) Schottky-type devices and on blend systems based on fullerene derivatives and polythiophenes.[20−23] RR-P3ATs are widely used and studied in a range of electronic applications chiefly due to their high charge carrier mobility stemming from their semicrystalline nature. Crystallinity and hence charge mobility in RR-P3ATs strongly depends on the degree of regioregularity of the polymer.[44] The nature of the alkyl substituent plays an important role in determining the electronic and physical properties. For instance, the side chain length directly affects the solubility of the polymer, its ability to form interchain order in solution-deposited films and the interchain stacking distance in these films.[24,25] Additionally, electronic energies, surface tension, and thermal properties (e.g., glass transition and recrystallization temperatures) can vary depending on the alkyl substituent.[25−27] When P3ATs are blended with another polymer, we can expect a range of interacting effects as the side chain is varied.[20,21] In particular, important properties for photovoltaic devices such as the effective charge mobility and the degree of phase separation can be tuned.[20,21,28] We therefore hope to optimize photovoltaic device performance by appropriate choice of P3AT and suitable processing conditions. In this manuscript the relevant properties (energy levels, thermal and photophysical properties) of the unblended P3ATs used in this study are presented, followed by a systematic study of the influence of alkyl chain length on the device physics and photovoltaic performance of P3AT/F8TBT blends. We find that P3HT produces the highest efficiency devices because of a combination of favorable energy level offsets that drive charge generation and separation, and a moderate glass-transition temperature that facilitates the optimization of the nanomorphology.

## Experimental Details

**1. Materials and Film/Device Preparation.** All substrates (Spectrosil quartz glass or ITO-coated sodium silicate glass) were cleaned by sonication in methanol, acetone and isopropanol (20 min each), followed by oxygen plasma etching (250 W, 10 min). For photovoltaic device preparation the cleaned ITO-glass substrates were additionally coated with a 70 nm thick film of PEDOT:PSS via spin-casting in air from sonicated and filtered (0.2 $\mu$m) colloidal solution (BaytronP, H.C. Starck GmbH, PSS-enriched to give a PEDOT-to-PSS ratio of 1:16), followed by annealing (250 °C, 10 min, $N_2$) prior to further processing. The photoactive polymers were used without further purification, either pure or in 1:1 ratio (by weight) blends. The acceptor polymer F8TBT was supplied by Cambridge Display Technology Ltd. with a molecular weight ($M_W$) of 55 kg mol$^{-1}$. All poly(3-alkylthiophenes) were supplied by Rieke Metals Inc., namely poly(3-butylthiophene) (P3BT) (138 kg mol$^{-1}$, regioregularity 93%, electronic grade), poly(3-hexylthiophene) (P3HT) (46 kg mol$^{-1}$, regioregularity 93%, electronic grade), poly(3-octylthiophene) (P3OT) (194 kg mol$^{-1}$, regioregularity 93%, electronic grade) and poly(3-decylthiophene) (P3DT) (222 kg mol$^{-1}$, regioregularity 93%, electronic grade). The specifications for these polymers were especially requested from the supplier for each batch. We note that there is a large difference in the molecular weights of the P3HT used and the other polythiophenes. To account for potential molecular

(14) Veldman, D.; Ipek, O.; Meskers, S. C. J.; Sweelssen, J.; Koetse, M. M.; Veenstra, S. C.; Kroon, J. M.; van Bavel, S. S.; Loos, J.; Janssen, R. A. J. *J. Am. Chem. Soc.* **2008**, *130*, 7721–7735.
(15) McNeill, C. R.; Westenhoff, S.; Groves, C.; Friend, R. H.; Greenham, N. C. *J. Phys. Chem. C* **2007**, *111*, 19153–19160.
(16) Jaczewska, J.; Budkowski, A.; Bernasik, A.; Moons, E.; Rysz, J. *Macromolecules* **2008**, *41*, 4802–4810.
(17) McNeill, C. R.; Watts, B.; Thomsen, L.; Belcher, W. J.; Greenham, N. C.; Dastoor, P. C.; Ade, H. *Macromolecules* **2009**, *42*, 3347–3352.
(18) Moons, E. *J. Phys.: Condens. Matter* **2002**, *14*, 12235–12260.
(19) Peet, J.; Senatore, M. L.; Heeger, A. J.; Bazan, G. C. *Adv. Mater.* **2009**, *21*, 1521–1527.
(20) Camaioni, N.; Casalbore-Miceli, G.; Catellani, M.; Luzzati, S.; Porzio, W. *Materials Science and Engineering C* **2001**, *15*, 261–263.
(21) Nguyen, L. H.; Hoppe, H.; Erb, T.; Günes, S.; Gobsch, G.; Sariciftci, N. S. *Adv. Funct. Mater.* **2007**, *17*, 1071–1078.
(22) Al-Ibrahim, M.; Roth, H.-K.; Schroedner, M.; Konkin, A.; Zhokhavets, U.; Gobsch, G.; Scharff, P.; Sensfuss, S. *Org. Electron.* **2005**, *6*, 65–77.
(23) Gadisa, A.; Oosterbaan, W. D.; Vandewal, K.; Bolsee, J.-C.; Bertho, S.; D'Haen, J.; Lutsen, L.; Vanderzande, D.; Manca, J. V. *Adv. Funct. Mater.* **2009**, *19*, 1–7.
(24) Sirringhaus, H. *Adv. Mater.* **2005**, *17*, 2411–2425.
(25) Ewbank, P. C.; Laird, D.; McCoullough, R. D. Regioregular Polythiophene Solar Cells: Material Properties and Performance. In *Organic Photovoltaics: Materials, Device Physics, and Manufacturing Technologies*; Brabec, C., Dyakonov, V., Scherf, U., Eds.; Wiley-VCH: Weinheim, Germany, 2008.
(26) Malik, S.; Nandi, A. K. *J. Polym. Sci., Part B: Polym. Phys.* **2002**, *40*, 2073–2085.
(27) Chen, S.-A.; Ni, J. M. *Macromolecules* **1992**, *25*, 6081–6089.
(28) Park, Y. D.; Kim, D. H.; Jang, Y.; Cho, J. H.; Hwang, M.; Lee, H. S.; Lim, J. A.; Cho, K. *Org. Electron.* **2006**, *7*, 514–520.

weight effects we have also used P3BT, P3OT and P3DT from another supplier with molecular weights in the range 46−55 kg $mol^{-1}$ and observed very similar results to those presented here (see the Supporting Information). Furthermore, it should be noted that the strongest molecular weight effects for P3HT have been found to occur for $M_W < 20$ kg $mol^{-1}$.[29] All solutions were prepared from anhydrous *o*-xylene (Sigma-Aldrich) at 70 °C (to enhance solubility) and spin-coated from hot solution either onto Spectrosil quartz substrates for photophysical characterization and AFM imaging or onto PEDOT:PSS-coated ITO on glass for device fabrication. Solution and film preparation was carried out under nitrogen. The semiconducting film thickness was 60−70 nm. Devices were completed by evaporation of a 100 nm aluminum cathode, followed by annealing. All annealing was carried out for 10 min under nitrogen; the annealing temperature was optimized separately for each materials system. These optimum annealing temperatures were found to be 180 °C for P3BT, 130 °C for P3HT, 100 °C for P3OT, and 60 °C for P3DT blend devices. To avoid environmental influences during testing, devices were encapsulated (using an epoxy-glass combination) after preparation. Film samples on Spectrosil were kept under nitrogen atmosphere until characterization.

**2. Methods.** Imaging was performed using atomic force microscopy (Veeco Dimension 3100 AFM, operated in tapping mode). Phase transitions of the polymers as a function of temperature were recorded using DMA (dynamic mechanical analysis) (TA Instruments Q800 DMA) in the temperature range 20 to 200 °C at a heating rate of 2 °C/min and a frequency of 1 Hz and via DSC (differential scanning calorimetry) (TA Instruments Q2000 DSC) in the temperature range 50−200 °C at a heating/cooling rate of 10 °C/min. HOMO (highest occupied molecular orbital) level determination was carried out via cyclic voltammetry, using a three-electrode cell (BAS Inc.), consisting of a platinum disk working electrode (diameter 1.6 mm), a platinum wire counter electrode and a Ag/AgCl reference electrode. Experiments were run by computer-controlled potentiostat (Reference 600 potentiostat/galvanostat/ZRA, Gamry Instruments) at a scan rate of 100 mV/s. For each measurement 2 $\mu$L of the particular polymer solution (10 mg/mL) was drop-cast onto the freshly polished platinum working electrode and allowed to dry. The scans were performed in an electrolyte solution of 0.1 M tetrabutylammonium hexafluorophosphate (TBAH, supplied by Fluka) in anhydrous propylene carbonate (Sigma Aldrich). Film thickness was measured using a stylus profilometer (Veeco Dektak 6M). For device characterization, external quantum efficiency (EQE) was measured as a function of wavelength, using a monochromatic light source (100 W tungsten filament lamp, passed through a monochromator) at intensities of less than 1 mW/$cm^2$, with a final spot size smaller than the device active area. The short-circuit current was recorded with a Keithley 237 source measure unit (SMU). Incident light intensity was continuously monitored during measurement and calibrated by a Hamamatsu S8746−01 photodiode. Current−voltage characteristics were recorded in the dark and under the same illumination as used for EQE measurements using the Keithley 237 SMU. Current−voltage characteristics were also acquired under simulated solar conditions (intensity equivalent to 100 mW/$cm^2$, AM 1.5G, after correction for spectral mismatch) using a solar simulator light source (Oriel 81160−1000) calibrated to a silicon reference cell. Optical absorbance was measured on polymer films deposited on Spectrosil quartz glass with a UV/vis spectrophotometer (Hewlett-Packard HP 8453). Photoluminescence spectra and quantum efficiencies were measured in a nitrogen-purged integrating sphere under argon ion laser excitation at 515 nm at room temperature. Light was detected with an Oriel InstaSpec IV spectrograph. Photoluminescence quantum efficiencies were calculated as described by de Mello et al.[30] Charge-transport properties of P3AT:F8TBT blends were studied by space-charge limited current (SCLC) measurements on double-carrier devices, fabricated similarly to photovoltaic devices as described above. The effective field-dependent majority charge carrier mobility therefore was determined by nonlinear least-squares fitting of the experimental dark-current−voltage data to the modified Mott-Gurney equation.[31] Because the aluminum electrode forms a blocking contact for the injection of electrons, these devices can be considered to be hole-dominated.

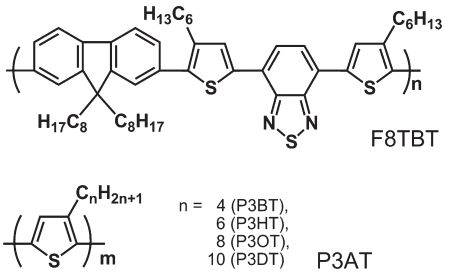


**Figure 1.** Chemical structures of F8TBT and P3ATs.

## Results and Discussion

**1. Photophysics and HOMO/LUMO Level Determination of P3ATs and F8TBT.** The chemical structures of the photoactive polymers used in this study, the acceptor F8TBT and the donor P3AT are displayed in Figure 1. The side-chain length of the P3AT increases following P3BT < P3HT < P3OT < P3DT according to the number of carbon atoms in the alkyl chain being $n = 4, 6, 8$, or 10, respectively. Analysis of the optical absorption of P3ATs or P3AT-containing blends is a useful tool to determine the degree of order and the internal structure of P3AT in films.[32] The absorption profile of regioregular P3AT films is characterized by a mixture of well-defined vibronic peaks, arising from absorption by weakly interacting H-aggregates, and a broader featureless absorption profile that is blue-shifted relative to the aggregate absorption due to the presence of disordered or "solution-like" chains.[33] The prominence of the vibronic bands in the absorption profile can thus be used to assess the degree of order in P3AT films.[33] We note that the difference in total absorption strength of the different neat P3AT films or their blends is not significant. The according unnormalized graphs are given as Supporting Information. Figure 2a shows the normalized optical absorption spectra of the unblended polythiophene films and Figure 2b that of their 1:1 blends with F8TBT (after annealing), with the spectrum of pure F8TBT shown for

(29) Kline, R. J.; McGehee, M. D.; Kadnikova, E. N.; Liu, J.; Frechet, J. M. J.; Toney, M. F. *Macromolecules* **2005**, *38*, 3312–3319.
(30) de Mello, J. C.; Wittmann, H. F.; Friend, R. H. *Adv. Mater.* **1997**, *9*, 230–232.
(31) Murgatroyd, P. N. *J. Phys. D: Appl. Phys.* **1970**, *3*, 151–156.
(32) Spano, F. C. *Chem. Phys.* **2006**, *325*, 22–35.
(33) Clark, J.; Silva, C.; Friend, R. H.; Spano, F. C. *Phys. Rev. Lett.* **2007**, *98*, 206406.

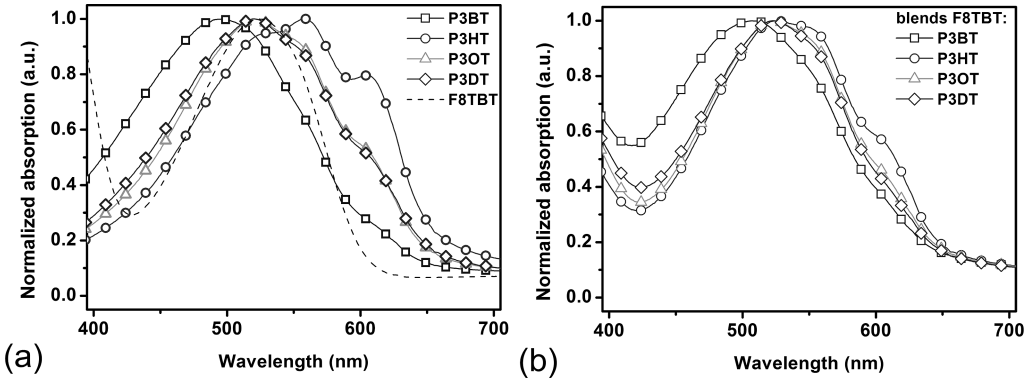


**Figure 2.** Normalized optical absorption of thin films of (a) pure P3ATs or F8TBT and (b) P3AT:F8TBT blends after optimum annealing.

comparison. Considering the unblended P3AT films first, it can be seen that the spectrum of P3HT (medium side-chain length) shows the strongest red-shift and the most prominent vibronic features compared to the other P3ATs, with the maximum in absorption found at 531 nm. The absorptions of P3OT and P3DT (longer side-chain) are quite similar but blue-shifted compared to that of P3HT, both showing maximum absorption around 520 nm and less distinctive vibronic features. P3BT with the shortest side-chain length shows only very weak vibronic features and the maximum absorption is highly blue-shifted, found at around 495 nm. Apart from the P3HT absorption, which is obviously more red-shifted because of a significantly higher degree of order compared to the P3OT and P3DT films, the observed trend in results is similar to that reported in the literature.[34] The obvious difference in morphology and hence in intermolecular coupling of pure P3AT films is probably related to the film forming properties of the materials during processing. This issue has been addressed recently by Oosterbaan et al.[46] Although unblended P3AT films generally have a high degree of crystallinity despite the relatively short drying time of the film, in blends the ability to form crystalline domains is disturbed by the presence of another immiscible polymer, in our case the amorphous F8TBT. The resulting absorption spectra of as-spun blends (not shown) therefore are a superposition of the pure F8TBT absorption spectrum (as shown in Figure 2a) and the solution-like absorption spectrum of the corresponding P3AT. The as-spun blend spectra show minimal vibronic features and are highly blue-shifted. By application of optimum postdeposition annealing of the film at certain temperatures (see below) the P3AT order within the blend is increased, as shown for P3HT:F8TBT blends by McNeill et al..[35] Considering the resulting absorption spectra of the annealed P3AT:F8TBT films (Figure 2b), the P3HT blend again shows the most distinctive vibronic features, with the vibronic features of the P3OT and P3DT blends less prominent. The maximum absorption for these three blends is at 524 nm, which corresponds to the absorption maximum of pure F8TBT. The optical absorption of the P3BT blend is significantly different, being featureless and blue-shifted with the maximum located at 501 nm. Table 1 shows the optical bandgaps, $E_g$, of the polymers used, taken from the low-energy absorption onset. The bandgap of F8TBT, about 2.0 eV, is slightly larger than those of the polythiophenes, which are all found around 1.9 eV.

**Table 1. Cyclic Voltammetry Data, Optical Bandgap and HOMO and LUMO Levels of the Acceptor F8TBT and the Donors P3BT, P3HT, P3OT, and P3DT**

| material | $E_{ox\ onset}$ vs Ag/AgCl (V) | HOMO (eV) | $E_{g\ optical}$ (eV) | LUMO (eV) |
|---|---|---|---|---|
| F8TBT | +1.3 | −5.6 | 2.0 | −3.6 |
| P3BT | +0.8 | −5.1 | 1.9 | −3.3 |
| P3HT | +0.5 | −4.9 | 1.9 | −3.1 |
| P3OT | +0.9 | −5.2 | 1.9 | −3.4 |
| P3DT | +0.9 | −5.3 | 1.9 | −3.5 |

The ionization potential and electron affinity of donor and acceptor materials are important parameters for photovoltaic operation, but values for the P3ATs differ significantly between different literature reports. We have therefore used cyclic voltammetry to estimate the HOMO and LUMO (lowest unoccupied molecular orbital) energies of our materials. The HOMO level (ionization potential) is calculated from the oxidation onset via

$$E_{HOMO} = (E_{ox-onset(vs\ Ag/AgCl)} - E_{redox(Fc/Fc^{+}vs\ Ag/AgCl)}) - 4.8\ eV$$

(using the ferrocenium/ferrocene ($Fc^+$/Fc) redox couple with a potential of 4.80 eV relative to vacuum as the reference potential).[22,36] The oxidation onsets of F8TBT and the four P3ATs and the corresponding HOMO levels calculated in this way can be found in Table 1. The LUMO level (electron affinity) can in principle be calculated using the reduction onset, however these measurements were difficult to perform reliably for some of our materials. We have therefore estimated the electron affinity simply by subtraction of the band gap energy $E_g$ from the ionization potential following $E_{LUMO} = E_{HOMO} - E_g$. There are significant uncertainties inherent in this

(34) McCullough, R. D.; Lowe, R. D.; Jayaraman, M.; Anderson, D. L. *J. Org. Chem.* **1993**, *58*, 904–912.
(35) McNeill, C. R.; Halls, J. J. M.; Wilson, R.; Whiting, G. L.; Berkebile, S.; Ramsey, M. G.; Friend, R. H.; Greenham, N. C. *Adv. Funct. Mater.* **2008**, *18*, 2309–2321.
(36) Kucur, E.; Riegler, J.; Urban, G. A.; Nann, T. *J. Chem. Phys.* **2004**, *120*, 1500–1505.

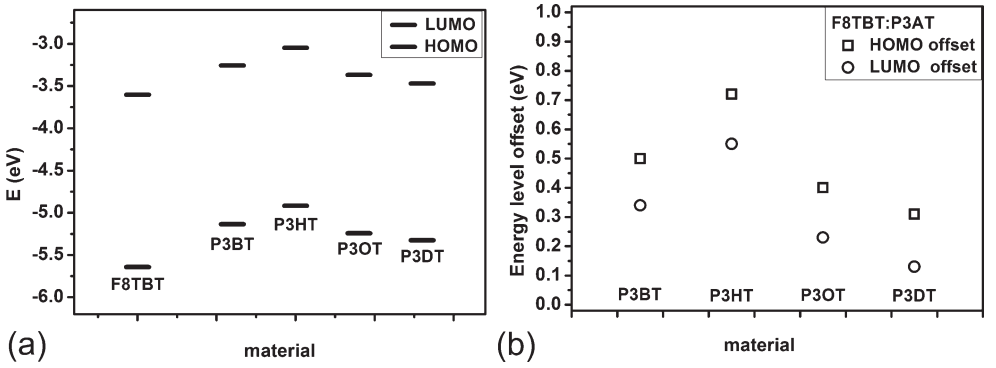


**Figure 3.** (a) HOMO and LUMO level energies of F8TBT and poly(3-alkylthiophenes) as determined by cyclic voltammetry and optical absorption, (b) energy level offsets between F8TBT and different P3ATs.

method, for example due to the neglect of excitonic binding energy and other screening effects. Nevertheless the trends between different materials are of interest, as shown in Table 1 and Figure 3a. The energy offsets in HOMO and LUMO levels between donor and acceptor determine the internal driving force for charge transfer in a blend and thus control the performance of an organic photovoltaic device. To achieve charge transfer, the offset energy must be sufficient to place the charge-transfer state lower in energy than the intrachain exciton. Offsets of 0.4 eV, comparable with the exciton binding energy, have typically been assumed to be required,[4] but offsets as low as 0.1 eV have recently been found to be sufficient,[37] consistent with a significant residual Coulombic binding energy in the charge-transfer state. Figure 3b shows the estimated HOMO and the LUMO offset energies of all four P3ATs relative to the F8TBT HOMO and LUMO respectively. For all polymers the HOMO offset exceeds the LUMO offset. It can be seen that P3HT shows by far the largest energy offsets, followed in sequence by P3BT > P3OT > P3DT. It should be mentioned that the found energy level difference between the four P3ATs cannot be caused exclusively by the molecular structure of the polymers, but rather by intermolecular coupling. According to a review paper by Jean Roncali,[45] the HOMO and LUMO levels of conjugated polymers are mainly influenced by five factors. Four of them have their origin in the bare molecular structure: (1) bond length alternation, (2) mean deviation from planarity, (3) aromatic resonance energy of the cycle on the monomer unit, (4) electron releasing or withdrawing substituents. The fifth factor is intermolecular coupling in the solid state. For the comparison of P3AT energy levels, due to identical polymer backbones and reactive terminal groups, only factors 2 and 5 are relevant. The mean deviation from planarity can be an issue in P3ATs. Backbone torsion, which causes loss of conjugation length, increase in the ionization energy, and widening of the HOMO−LUMO energy gap, depends on the side chain length and type (e.g., steric hindrance). However, we believe that this effect is rather minor in the narrow range of alkyl groups investigated ($n$ = 4, 6, 8, 10). The intermolecular coupling in P3AT solid films on the other hand might have strong influence on the energy levels as a consequence of film forming properties of the materials during processing. This issue has been addressed recently by Oosterbaan et al.[46]

Photoluminescence measurements can be used to estimate the efficiency of exciton dissociation by quantifying the residual luminescence in the blend compared to the pristine materials. Qualitative comparison of the shape of the blend photoluminescence (PL) spectrum with that of the pure materials can also assist analysis of photophysical processes in the blend. Figure 4 shows the photoluminescence intensities and efficiencies of the pure P3ATs, pure F8TBT and their blends, excited at 515 nm. Considering the PL spectra of the pure polymers first, it can be seen that the F8TBT PL spectrum is featureless and has its maximum at about 695 nm. The PL spectra of the pure polythiophenes are characterized by two vibronic peaks (poorly resolved). The maximum emission of P3HT is found at 723 nm and is blue-shifted compared to the other P3ATs. P3OT and P3DT both show an emission maximum at around 735 nm; P3DT shows the most distinctive vibronic features of all the P3ATs investigated. P3BT shows a broad featureless emission, slowly falling toward longer wavelengths, with an emission maximum at 743 nm. Regarding the remaining photoluminescence of the annealed blends it can be seen that blends with P3BT, P3OT, and P3DT have their emission maximum at around 679 nm (close to the F8TBT maximum), whereas the P3HT blend shows its maximum emission at 724 nm (identical to that of unblended P3HT). In general, though, it is difficult to assign the emission to either F8TBT or P3AT, because the P3ATs are so sensitive to the degree of ordering in the regions where the excitons emit. A more quantitative view is given by the photoluminescence quantum efficiency (PLQE) data displayed in Figure 4c. The PLQE of pure F8TBT is around 34% (not shown). It can be seen that the PLQE of pure P3BT is 2.7%, the lowest among the P3ATs used, whereas those of the other P3ATs are between 7.1 and 9.3%. Considering the efficiencies of the remaining PL of the annealed blends, a different trend is visible. Here the blends of P3BT, P3HT, and P3OT show almost equal PLQEs,

(37) Veldman, D.; Meskers, S. C. J.; Janssen, R. A. J. *Adv. Funct. Mater.* **2009**, *19*, 1939–1948.

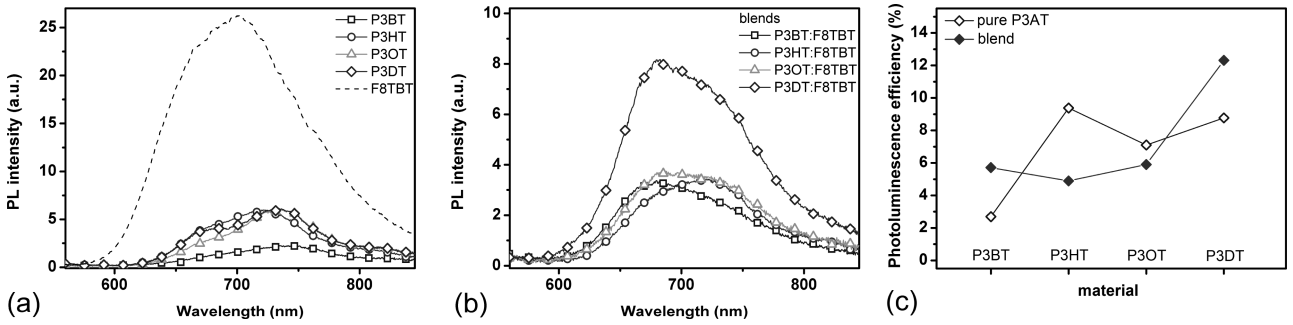


**Figure 4.** Photoluminescence spectra of (a) pure P3ATs and F8TBT, and (b) P3AT:F8TBT blends. (c) Photoluminescence efficiency of pure P3ATs and P3AT:F8TBT blends. The PLQE of pure F8TBT (not displayed) is 34%.

between 4.9 and 5.7%, whereas P3DT blends show the highest remaining PL with PLQEs of about 12%.

**2. Thermal Characteristics of P3ATs and F8TBT.** Temperature-dependent phase transitions in polymers are strongly dependent on the state of the polymer, semicrystalline or amorphous, and depend on the substituted groups or side-chains.[38] DSC and DMA provide two independent methods to determine phase transitions in polymers by scanning changes either in the thermal energy uptake or in the mechanical damping of the material. Amorphous polymers like F8TBT do not tend to show clear transitions in DSC and DMA scans; rather they gradually change from the glassy state into the liquid state by passing through a rubbery region. Semicrystalline polymers like P3ATs consist of an ordered and a disordered phase and therefore show superposed transitions of both phases.[39] DSC can only detect phase transitions that are accompanied by a clear endothermic or exothermic peak such as melting or crystallization and effects accompanied by changes in heat capacity of the material (visible as steplike changes in heat flow), determining, for example, glass transitions. DMA is a much more sensitive method, which can also detect less prominent transitions, but the origin of these transitions is generally harder to attribute. Transitions that may be observed with DMA include the glass−rubber−liquid transition, the crystalline−liquid transition, side-group/side-chain relaxation, and main-chain twisting.[27,40,41] Here, the transition temperatures for F8TBT and the four P3ATs studied have been extracted from DSC thermograms and from DMA damping. All designated transition temperatures found between 20 and 200 °C are listed in Table 2, excluding the polymer (main-chain) melting points. For F8TBT three transitions are found with DMA and one with DSC. Since F8TBT is amorphous and possesses hexyl and octyl side chains, two of the transitions are assigned to side-chain relaxations, $\alpha_2$ from the octyl chain and $\alpha_3$ from the hexyl chain. In DSC, only the hexyl chain relaxation is found, at around 125 °C. The lowest DMA transition $\alpha_1$ cannot be classified. For the polythiophenes, it can be seen that each P3AT except for P3DT exhibits at least two transitions in DMA and one in DSC. From the DMA results, all transition temperatures decrease with increasing side-chain length, consistent with earlier studies.[27] For identification of the origin of these transitions the structure of the P3ATs studied has to be taken into account. Only regioregular P3ATs were used, which are semicrystalline and so consist of an ordered and a disordered phase. Furthermore, just one type of side-chain is present, namely butyl, hexyl, octyl, or decyl groups. Two transitions are expected to be observed from relaxation of the alkyl chain: one from the disordered phase at lower temperature (because of the higher free volume in amorphous structures) and one from the ordered phase at higher temperature. Examining the DMA transition data of the P3ATs in Table 2, the $\alpha_3$ transitions are attributed to the relaxation of the alkyl chains within the crystalline parts, and correspond to the glass transition temperature. The $\alpha_2$ transition is attributed to the relaxation of the alkyl chains in the disordered P3AT regions, a transition that is sometimes referred to as a "second glass transition". In the case of P3BT, no $\alpha_3$ transition is found as it is likely to be outside the temperature range used (that is, above 200 °C). The origin of the $\alpha_1$ transitions is unclear. The data obtained by DSC support the DMA results only in the case of P3HT and P3OT, verifying the $\alpha_3$ glass transitions. For P3BT, the DSC transitions do not correspond to the DMA results, being located at different temperatures. DSC thermograms of P3DT also did not show any discernible transitions. To summarize the thermal characterization studies, the glass-transition temperature (defined as the

**Table 2. DMA and DSC Temperature Data of Phase Transitions in F8TBT and Poly(3-alkylthiophenes) P3BT, P3HT, P3OT, and P3DT ($\alpha_1$, $\alpha_2$ and $\alpha_3$ Number Different Phase Transitions)**

| material | transition peak temperatures DMA (°C) | | | transition temperatures DSC (°C) | |
|---|---|---|---|---|---|
| | $\alpha_1$ | $\alpha_2$ | $\alpha_3$ | | |
| F8TBT | 69 | 100 | 128 | 123 | |
| P3BT | 40 | 78 | | 124 | 180 |
| P3HT | 34 | 69 | 138 | 142 | |
| P3OT | | 55 | 96 | 94 | 109 |
| P3DT | | 44 | 69 | | |

(38) Donth, E.-J. In *The Glass Transition: Relaxation Dynamics in Liquids and Disordered Materials*; Wang, Z. M., Jagadish, C., Hull, R., Osgood, R. M., Parisi, J., Warlimont, H., Eds.; Springer Series in Material Science; Springer: New York, 2001; Vol. *48*.
(39) Shaw, M. T.; MacKnight, W. J. *Introduction to Polymer Viscoelasticity*, 3rd ed.; Shaw, M. T., Ed.; John Wiley & Sons: New York, 2005.
(40) Yazawa, K.; Inoue, Y.; Yamamoto, T.; Asakawa, N. *J. Phys. Chem. B* **2008**, *112*, 11580–11585.
(41) Liu, S. L.; Chung, T. S. *Polymer* **2000**, *41*, 2781–2793.

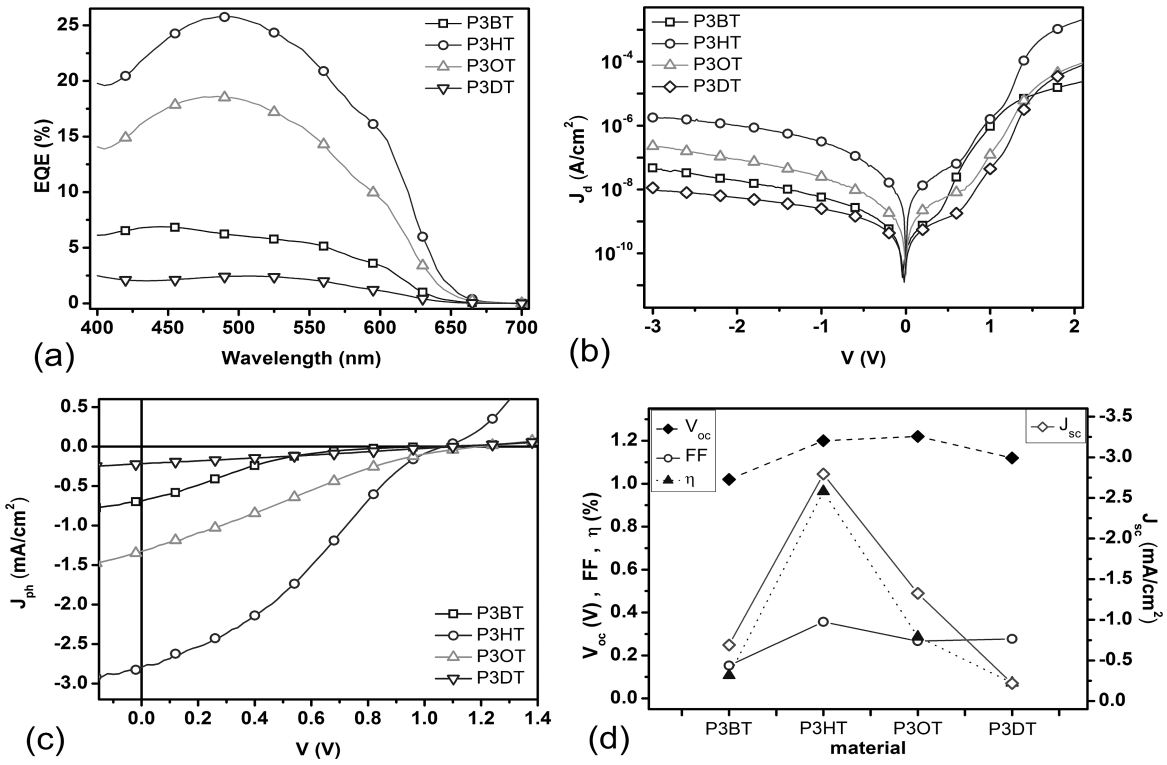


**Figure 5.** Device characteristics of the optimized P3AT:F8TBT solar cells, (a) external quantum efficiency, (b) dark current density, (c) photocurrent density (under AM1.5G illumination at 100 mW/cm$^2$). (d) Comparison of the solar cell key values $J_{sc}$, FF, $V_{oc}$, and PCE ($\eta$).

temperature where all side chains are mobile) was measured to be 140 °C for P3HT, 100 °C for P3OT and 70 °C for P3DT. For P3BT the glass-transition temperature is not clear, possibly located at around 180 °C (as detected in DSC) or even higher. Knowledge of the glass transition temperatures of F8TBT and the P3ATs will be useful the following sections in helping to understand the optimum annealing temperature observed for each P3AT:F8TBT blend solar cell. In P3ATs, annealing to the glass-transition temperature promotes recrystallization, whereas in F8TBT, it mainly controls the polymer mobility (increase in domain size).

**3. Photovoltaic Characteristics.** P3AT:F8TBT blend solar cells have been prepared using 1:1 ratio of F8TBT and either P3BT, P3HT, P3OT or P3DT. First the optimum annealing temperatures for gaining best device performance have been investigated for each P3AT:F8TBT combination. Optimum annealing temperatures of 130, 100, and 60 °C were determined for P3HT, P3OT, and P3DT blend devices, respectively. In the case of P3BT, device performance was found to increase monotonically with annealing temperature but appeared to saturate around 180 °C, so this was set as "optimum temperature". The optimum annealing temperatures for P3AT:F8TBT devices are found close to the appropriate P3AT glass-transition temperature (see above), except for P3BT blends. In the case of P3BT, no clear glass transition was found in our measurements. Next, we have focused on the comparison between the properties of optimized P3AT:F8TBT devices containing different P3ATs. Figure 5 shows the typical device characteristics of each P3AT:F8TBT blend solar cell used in this study. Looking at the external quantum efficiency (EQE) results of the four systems (Figure 5a) (recorded at low light intensity), it can be seen that P3HT devices show the highest EQEs of around 26%, followed by P3OT with peak EQE of around 19%. The EQEs of the other two blend systems were significantly lower at around 7% for P3BT and less than 3% for P3DT devices. The dark current characteristics of the devices are shown in Figure 5b. The P3HT blend devices show the highest dark current density ($J_d$) of all the P3AT blends studied, followed by the P3OT blend and then the P3BT blend with the P3DT device showing the lowest $J_d$. This trend may be due to different charge mobilities in these blends. A similar trend can be seen regarding the photocurrent density of the four blend systems (Figure 5c), recorded under simulated solar conditions (100 mW/cm$^2$, AM 1.5G). Here the P3HT:F8TBT device shows by far the highest short-circuit current density and power conversion efficiency, followed by the P3OT:F8TBT, P3BT:F8TBT, and P3DT:F8TBT devices. We note that the s-shape of the photocurrent curves is associated with a charge extraction barrier in forward bias. We believe this effect is due to vertical phase separation in our blends.[35] Naturally, the extent of this effect varies with alkyl-chain length due to the different material properties of the polymers. The essential device parameters extracted from solar simulator measurements, namely the short-circuit current ($J_{sc}$), the open-circuit voltage ($V_{oc}$), the fill factor (FF) and the power conversion efficiency ($\eta$) of the four P3AT:F8TBT systems, are displayed together in Figure 5d. Although the energy level determination for the donor and acceptor materials (see above) would

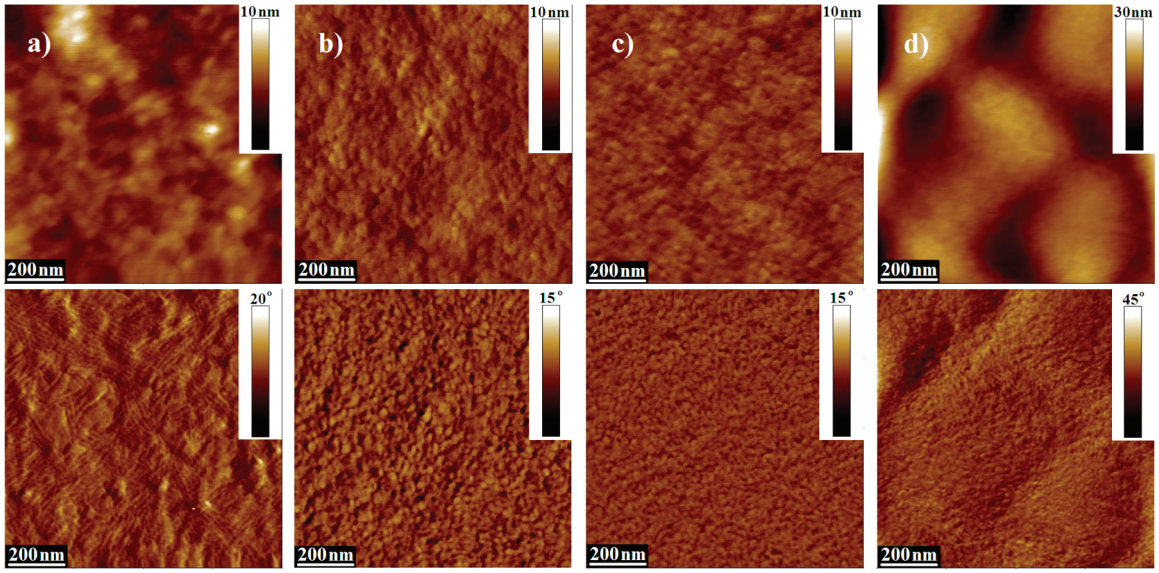


**Figure 6.** AFM height (top) and phase (bottom) images of the different blend systems, annealed under optimum conditions: (a) P3BT, (b) P3HT, (c) P3OT, and (d) P3DT blend.

suggest the lowest $V_{oc}$ for P3HT devices and higher values for the other blends, the open-circuit voltages for P3HT, P3OT, and P3DT are found to be quite similar, around 1.2 V, with P3OT showing a slightly higher value. P3BT devices show a considerably lower $V_{oc}$ of about 1.0 V. There is no obvious correlation between the measured open-circuit voltages and the maximum open-circuit voltages predicted from the energy levels in Figure 3a. Regarding the photocurrent fill factors of the four systems, again the values for P3HT, P3OT and P3DT are quite similar at around 35%, with P3HT being slightly higher. P3BT devices in contrast show a notably lower fill factor of 15% suggesting a very poor charge separation efficiency at low fields in this combination. Considering the results for the power conversion efficiency of the four P3AT systems, it is found that its trend follows the changes in short-circuit current quite closely. Both device parameters are the highest by far for P3HT devices, showing a $J_{sc}$ of around 2.8 mA/cm$^2$ and $\eta$ of 1.0%. The next best results are shown by P3OT blends, achieving $J_{sc}$ of 1.3 mA/cm$^2$ and $\eta$ of 0.3%, considerably worse than for the P3HT devices. The values for the other two blends are even lower, giving $J_{sc}$ of 0.7 mA/cm$^2$ and $\eta$ of 0.1% for P3BT, and $J_{sc}$ of 0.2 mA/cm$^2$ and $\eta$ of 0.07% for P3DT devices.

**4. Morphology of P3AT:F8TBT Blends.** To gain more information about the morphology of P3AT:F8TBT blends after optimum annealing, AFM imaging (tapping mode) was used. Figure 6 shows the AFM topography (top) and phase images (bottom) of blends containing (a) P3BT, (b) P3HT, (c) P3OT, and (d) P3DT after annealing of each film at the optimum temperature. The surface morphology of the P3BT blend (a) shows a rather coarse structure with large domains of 50−100 nm size, infiltrated by a network of rodlike features of up to 100 nm length and 5−10 nm width. It is suggested that the large domains consist mainly of the amorphous F8TBT, whereas the rodlike material is crystalline P3BT. The P3HT (b) and P3OT (c) blend films

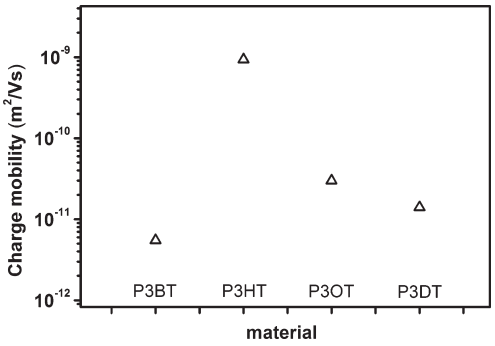


**Figure 7.** Zero-field charge mobility of the different blend systems, annealed under optimum conditions, extracted from space-charge-limited current analysis.

do not show rodlike features. Instead, a grainlike structure is observed, with much smaller domains of about 20−25 nm for the P3HT blend and an even finer structure for P3OT blend with domains around 10−15 nm diameter. For P3DT blends (d), these features were even smaller.

**5. Mobility.** The charge mobility of the ITO/PEDOT:PSS/P3AT:F8TBT/Al devices has been extracted by modeling the dark current under forward bias using the space-charge-limited expression

$$J_{SCL} = \frac{9}{8}\varepsilon\mu_0 e^{0.891\gamma\sqrt{V_{int}/L}}\frac{{V_{int}}^2}{L^3}$$

where $\mu_0$ is the zero-field mobility, $\gamma$ the field activation parameter, $J_{SCL}$ the current density, $\varepsilon$ the permittivity, $V_{int}$ the internal voltage, and $L$ the film thickness. This approach provides a reasonable estimation for the mobility of the major charge carrier within the blend. Because of the much higher barrier for injection of electrons into the F8TBT LUMO from the Al electrode compared to the injection of holes into the P3HT HOMO from PEDOT:PSS, these devices will be hole-dominated under forward bias. Therefore, the fitted mobilities are likely to reflect

the hole mobilities in the P3AT:F8TBT blends. The results of this fitting are displayed in Figure 7 (for further details, see the Supporting Information). The zero-field hole mobility of the P3HT:F8TBT blend has been determined to be $1 \times 10^{-9}$ m$^2$/(V s), consistent with previous measurements.[40−43] The hole mobilities of the other P3AT blends are much lower, with the P3OT and P3DT blends having a mobility of around $2 \times 10^{-11}$ m$^2$/(V s). P3BT shows, despite its apparently highly ordered structure seen in AFM, the worst charge mobility of around $6 \times 10^{-12}$ m$^2$/(V s).

**6. Discussion.** The above results demonstrate that when a polythiophene is introduced into a P3AT:F8TBT blend the choice of the alkyl substituent attached to the polythiophene affects the photovoltaic device performance as well as optical and morphological properties. We find P3HT and F8TBT to be the best-matching donor−acceptor couple from the P3ATs studied. Even after extensive annealing temperature studies on each system to find the optimum temperature for maximum device performance of each material system, none of the other P3AT combinations were able to match the P3HT:F8TBT performance. This result can be understood in terms of the different photophysical, morphological, and thermal properties of the blends.

The PL data presented in Figure 4b show quenching of F8TBT luminescence in all P3AT blends. This can in principle occur either via charge transfer at the interface, or via energy transfer from F8TBT to P3AT followed by emission from the P3AT with lower efficiency. The quenching is weakest in P3DT blends. Because these P3DT annealed blends remain finely mixed, the significant residual emission suggests that charge transfer is not efficient in this blend, consistent with the small energy level offset found in this system Figure 3b. For the other blends, the measured energy level offsets combined with the observed PL quenching are consistent with efficient electron transfer for excitons reaching the heterojunction. It is also worth noting that the system with the best EQE is the blend which, according to Figure 3b, has the largest energy level offsets to drive charge transfer. It may be that the excess energy assists in subsequent charge pair separation, or that reducing the energy of the charge-transfer state prevents competing decay mechanisms from occurring. However, we believe that changes in morphology and charge-transport properties provide a sufficient explanation for the changes in device performance, as discussed below.

Considering the thermal properties of the polymers, the moderate glass-transition temperature ($T_g$) of P3HT seems to combine well with the thermal properties of F8TBT. We found that the effective $T_g$ of F8TBT was around 130 °C, with annealing above this temperature allowing the polymer a certain level of mobility, inducing a small degree of demixing and phase separation which is beneficial to device performance. Ideally, the temperature at which the polythiophene reorganizes should be similar to or lower than that of F8TBT. If the reorganization of the polythiophene that is necessary for high mobilities occurs at too high a temperature, this change in packing cannot occur without significant phase separation of the blend that is detrimental to device performance. This may explain the poor performance of P3BT:F8TBT devices that display rather coarse features in the AFM images. For the P3HT:F8TBT blend whose $T_g$ is closest to that of F8TBT (140 °C vs 130 °C), we find the highest crystallinity compared to the other annealed blends (seen from optical absorption) and an intermediate degree of phase separation (from the AFM images) with a length scale within the diffusion length of the excitons, explaining the good performance of these devices. When going further to longer side-chains such as in P3OT, its $T_g$ is lower than that of F8TBT (100 °C vs 130 °C). Consequently the crystallinity is good, but the phase-separated domains are significantly smaller because F8TBT is not yet sufficiently mobile at that temperature, leading to a morphology that hinders charge separation and transport. This effect is even worse for P3DT, with the longest alkyl chain of the P3ATs studied (60 °C vs 130 °C), with phases hardly observable. Annealing of P3OT and P3DT blends at higher temperatures should in principle allow further beneficial phase separation; however, for reasons that are not clear, in practice no further improvement in device performance is seen. In summary, from the morphological point of view, P3HT is the only suitable option for an efficient solar cell with F8TBT because of the strong dependence of glass-transition temperature on side-chain length.

The film morphology is expected to directly influence the charge mobility, via the crystallinity in the P3AT phase and via the development of percolation pathways through the phase-separated structure. The largest charge mobility is found in P3HT devices, which apparently provide both an adequate network of separated polymer phases and sufficient crystallinity of the P3HT phase for optimum charge mobility. The charge mobility then drops with further extension of the alkyl chain for P3OT and P3DT. However, in pure P3ATs, the degree of order rises with longer side chains, because the main chain is forced to stay planar and thiophene twisting is inhibited and so should increase charge mobility, but at the same time the chain packing density decreases with longer side chains, which causes a larger intermolecular hopping distance so the actual charge mobility is diminished.[22−28] For P3BT, the situation is different. Although crystalline rods are clearly visible within the annealed blend with AFM and crystalline P3BT should have higher mobility because of the short hopping distance

(42) Marsh, R. A.; McNeill, C. R.; Abrusci, A.; Campbell, A. R.; Friend, R. H. *Nano Lett*. **2008**, *8*, 1393–1398.
(43) McNeill, C. R.; Greenham, N. C. *Appl. Phys. Lett*. **2008**, *93*, 203310.
(44) Woo, C. H.; Thompson, B. C.; Kim, B. J.; Toney, M. F.; Fréchet, J. M. J. *J. Am. Chem. Soc*. **2008**, *130*, 16324–16329.
(45) Roncali, J. *Chem. Rev*. **1997**, *97*, 173–205.
(46) Oosterbaan, W. D.; Bolsee, J.-C.; Gadisa, A.; Vrindts, V.; Bertho, S.; D'Haen, J.; Cleij, T. J.; Lutsen, L.; McNeill, C. R.; Thomsen, L.; Manca, J. V.; Vanderzande, D. *Adv. Funct. Mater*. **2010**, *20*, 792–802.

between the conjugated main chains, the measured charge mobility in this blend is quite low. This may be explained by the high concentration of P3BT rods at the film surface (as seen in AFM), which suggests strong vertical phase separation, with F8TBT enrichment near the PEDOT:PSS interface and P3BT at the surface, favored by the respective surface energies of the components. This unfortunate geometry may reduce charge transport within the blend and cause lower effective charge mobility.

## Conclusions

We have studied the properties of P3ATs with different alkyl chains and their effects on photovoltaic device performance in blends with F8TBT. In particular, we have focused on the relationship between thermal properties, morphology and energy level alignment. P3HT:F8TBT gave the best device performance, caused by suitable energy level alignment of both polymers and optimum film morphology of the annealed blend. Shortening the alkyl chain (P3BT:F8TBT) requires high annealing temperatures to promote P3BT reorganization, which leads to coarse phase separation and limits device performance. P3OT:F8TBT shows reasonable performance, because the HOMO offset is sufficient and the film morphology (crystallinity, interconnectivity, and domain size) is suitable. We conclude that the best morphology is obtained when the P3AT has a glass-transition temperature similar to that of F8TBT.

**Acknowledgment.** We are grateful to Cambridge Display Technology Ltd. (CDT) for the supply of materials, to the Technology Strategy Board for funding as part of the OPALS (TP/K2512F) collaborative project with CDT and Molecular Vision Ltd., and to Dr. J. J. M. Halls, Dr. A. B. Doust, Dr. G. Pace, and Mr. T. J. K. Brenner for useful discussions. C.R.M. thanks the EPSRC for provision of an Advanced Research Fellowship (EP/E051804/1).

**Supporting Information Available:** Additional tables and figures (PDF). This material is available free of charge via the Internet at http://pubs.acs.org.